DOI: 10.1002/cphc.200800124

Interfacial Organization of Y-Shaped Rod–Coil Molecules Packed into Cylindrical Nanoarchitectures

Libin Liu, Jung-Keun Kim, and Myongsoo Lee*[a]

The behavior at the air/water interface and the structures of Langmuir–Blodgett monolayers at different surface pressures of rod–coil molecules, which consist of a Y-shaped rigid aromatic segment containing peripheral tetradecyloxy groups and a flexible poly(ethylene oxide) (PEO) chain with 17, 21, 34, or 45 repeating ethylene oxide units (Y17, Y21, Y34, and Y45), were investigated. For the Y21 and Y34 molecules, AFM images revealed two kinds of cylindrical nanoarchitectures formed upon compression. The nanostructured films were further investigated by UV/Vis and FTIR spectroscopy. The formation of the cylindrical nanoarchitectures was due to different tilting angles offered by the mismatch of the cross-sectional areas of the PEO chain and the benzene ring with attached alkyl chains, and the different PEO contents of the molecules. The multiple π–π stacking and hydrophobic interactions provide exceptional stability of the nanostructures and allow them to be preserved in the course of flipping. For the shortest PEO chain of the Y17 molecule, spontaneous aggregation occurred. The Y45 molecule revealed the formation of 2D circular domains caused by entanglement of the longest PEO chains and coiling at the air/water interface. In addition, an interesting vortical morphology was obtained for the Y21 molecule upon deposition of the film onto a mica substrate, which indicates that the substrate chemistry also has an effect on the morphologies during the film-transfer process.

1. Introduction

The interfacial behavior of amphiphilic molecules is an intriguing topic in the field of organized molecular films.[1] The control and understanding of the self-assembly behavior of amphiphilic molecules at surfaces have received considerable interest in recent years due to the ability of these molecules to spontaneously organize into ordered surface patterns.[1,2] Much effort has been devoted to monolayer or ultrathin films of amphiphilic copolymers containing the poly(ethylene oxide) (PEO) block,[3–6] due to its surface-active nature at the air/water interface. The nanosized structures can be easily controlled by varying different parameters, such as the relative chain length of the hydrophilic and hydrophobic blocks,[5a,7,8] the surface pressure,[9] and the concentration of the spreading solution.[8,10]

Asymmetric diblock copolymers, such as rod–coil molecules consisting of a rigid rodlike segment and a flexible coil segment, give rise to novel ordered structures.[12,13] However, there are only a few reports on the interfacial assembly of rod–coil molecules at the air/water interface.[14,15] Specially designed molecules with particular architectures related to sterically asymmetric fragments were shown to be capable of packing into organized nanostructures.[11,16] The orientational order of the rod block induced by two-dimensional (2D) geometrical restrictions and substrate chemistry also has an important effect on the self-assembled nanostructures.

Herein, we focus on the investigation of the interfacial behavior of amphiphilic Y-shaped rigid-rod–coil molecules at the air/water interface and the structures of the films transferred onto solid substrates. These molecules have been observed to self-assemble into a variety of liquid-crystalline structures in the solid state,[17] but their ability to organize into nanostructures at the air/water interface was not studied.

Experimental Section

Materials: The rod–coil molecules, which consist of a Y-shaped rigid aromatic segment containing peripheral tetradecyloxy groups and a flexible PEO chain with different molecular weights, are depicted in Figure 1 and were prepared as previously reported.[17] The Y-shaped molecules are abbreviated as Y17, Y21, Y34, and Y45 (the numbers representing the number of ethylene oxide units).

Langmuir–Blodgett (LB) Film Fabrication: The molecular films were fabricated by a LB technique on a KSV minitrough system (KSV Instruments Ltd.) equipped with two moving barriers and a Wilhelmy plate for measuring surface pressure. Between runs, the trough was cleaned with acetone and rinsed several times with Nanopure water (18.2 MΩ cm). Dilute molecule solution (40–120-μL, 0.2–1 mg mL^{-1}) in chloroform (HPLC grade) was deposited in 5–10 drops uniformly distributed on the Nanopure water surface and left to evaporate and spread evenly for 30 min. The spreading solvent concentrations showed no effect on the surface behavior of the molecules. The compression rate was kept at 5 mm min^{-1} until the desired surface pressure was reached. Highly polished [100] silicon wafers were cut into rectangular pieces (2×2 cm^2) and sonicated in Nanopure water for 10 min to remove silicon dust. The wafers were then chemically treated with piranha solution (30% concentrated hydrogen peroxide, 70% concentrated sulfuric acid; *hazardous solution!*) for 1 h to strip off any organic contaminants clinging to the silicon oxide surface and at the same time oxidize/hydroxylate the surface.[18] Finally, the wafers were abundantly rinsed with Nanopure water and dried at room temperature. For

[a] *L. Liu, J.-K. Kim, Prof. M. Lee*
Center for Supramolecular Nano-Assembly, Department of Chemistry
Yonsei University, Seoul 120-749 (Korea)
Fax: (+82) 2-393-6096
E-mail: mslee@yonsei.ac.kr

Supporting information for this article is available on the WWW under http://dx.doi.org/10.1002/cphc.200800124.

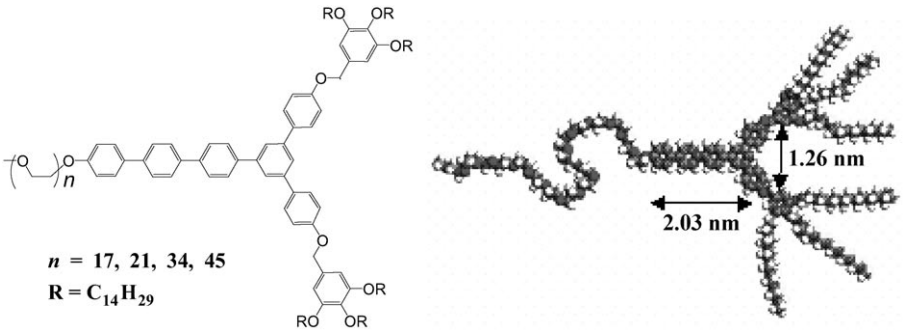

Figure 1. Chemical structure of the Y17, Y21, Y34, and Y45 molecules and the corresponding molecular model of Y17.

AFM measurements, the monolayer LB films of the Y-shaped molecules were transferred at a rate of 3 mm min^{-1} onto silicon wafers and freshly cleaved mica substrates at various surface pressures by the upstroke mode of the vertical dipping method. The typical transfer ratio was in the range of 0.8 to 1.0, which suggests a good film quality. For UV/Vis and FTIR spectral measurements, the floating films were transferred onto quartz and CaF_2 solid supports at selected surface pressures by the horizontal Langmuir–Schaefer method and with a certain number of depositions.

Characterization: The transferred films were air-dried in a desiccator for 24 h and subsequently scanned in tapping mode under ambient conditions with a Veeco NanoScope IIIa atomic force microscope (Digital Instruments, Inc., Santa Barbara, CA) using Nanosensors silicon probes (dimensions: $H = 3.5$–4.5, $W = 30$–40, $L = 115$–135 μm). An amplitude ratio of 0.95 and higher was employed to avoid monolayer damage.[19] The AFM scans were conducted at a scanning rate of 0.5–2 Hz for surface areas ranging from 10×10 μm^2 to 200×200 nm^2 and for several randomly selected locations with at least 40 different images collected for each specimen. All images were processed with a second-order flattening routine. The domain topography and the surface-area coverage were calculated from height histograms using the bearing analysis.[20] UV/Vis measurements of the films were performed at room temperature with a UV-1650PC spectrophotometer. FTIR measurements were recorded on an Equinox 55 FTIR spectrophotometer with an average of several hundreds scans.

2. Results and Discussion

2.1. Interfacial Behavior at the Air/Water Interface

All the Y-shaped molecules displayed amphiphilic behavior at the air/water interface. Typical surface-pressure-area isotherms of the molecules are presented in Figure 2. All the isotherms showed a steadily increasing surface pressure upon compression and were reversible up to modest surface pressures. The reversibility of the Langmuir monolayers was examined by repeating cycles of compression and expansion within the low-surface-pressure (< 2 mN m^{-1}) region. A minor hysteresis (5–10% surface area) observed in several particular cases for Y45 indicated partially irreversible behavior due to entanglement of the long PEO chains (not shown). This finding is consistent with the AFM images for Y45 deposition onto the substrate (see below).

For the Y17 molecule, there is a distinct gaseous region with zero surface pressure prior to the solid condensed region, whereas slightly increased surface pressures are observed for the Y21, Y34, and Y45 molecules. As compression continues, the curves present a pseudoplateau at a surface pressure of 8–10 mN m^{-1} and the following surface pressures increase sharply.

For the Y21, Y34, and Y45 molecules, at large molecular areas, the surface film is expanded. This region is typically known as the "pancake" region in which the PEO is believed to

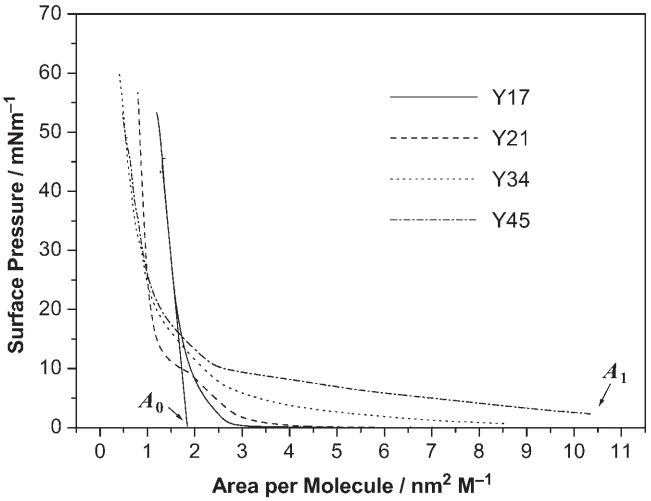

Figure 2. Pressure–area (p–A) curves of rod–coil molecules Y17, Y21, Y34, and Y45. A_0 = limiting cross-sectional surface area per molecule, A_1 = area of the onset of surface pressure.

adopt a pancake-like shape absorbed at the air/water interface.[21] Considering the affinity of PEO for the air/water interface and the similarity of our isotherms to those for linear copolymers in the literature,[22–24] we propose that the expanded region of the three isotherms represents a film of PEO at the surface. Due to its hydrophobicity, the aromatic segment in turn exists as small globules atop the PEO film. The volume fractions of the PEO chains, which were calculated from the known molar values for the bulk state[17] and the observed area of onset of the surface pressure (A_1), are shown in Table 1. The surface area per PEO unit (A_1/PEO unit) is within 0.22–0.25 nm^2, which is close to the surface area estimated for the PEO monomeric units oriented at the water surface and hydrogen-bonded with one to three molecules of water (0.28 nm^2 for the PEO monomeric unit with two water molecules).[24a,25] Thus, we suggest that the onset of the formation of the monolayer at the air/water interface is determined by the initial interaction of the hydrated PEO chains. The observed

Table 1. Observed area of onset of the surface pressure and the limiting cross-sectional surface area of the Y-shaped molecules.

Molecules	M_n	f_{PEO}[a]	Calculated molecular length[b] [nm]	A_1 [nm^2]	A_0 [nm^2]
Y17	2723.98	0.28	9.0	2.94	1.81
Y21	2900.19	0.32	10.2	4.52	1.13
Y34	3472.88	0.43	13.8	8.57	1.33
Y45	3957.46	0.50	17.1	10.42	1.36

[a] f_{PEO} is the volume fraction of PEO. [b] Molecular length was measured by the Corey–Pauling–Koltun (CPK) model.

pseudoplateau means that the transition of the PEO chains from the pancake conformation flattening on the water surface to a mushroom conformation dissolving into water occurred upon compression.[26]

In addition, careful observation shows that as the length of the PEO chain increases, the pseudoplateau pressures increase as well. The limiting cross-sectional surface area per molecule (A_0), calculated by the extrapolation of the steep rise in the surface pressure to a zero level, is shown in Table 1. On the basis of the molecular model, the surface area occupied by aromatic segments adopting a flat-on orientation was calculated to be about 2.56 nm^2. This value is higher than the limiting cross-sectional area of all the Y-shaped molecules, which indicates that the molecules contradict a flat-on orientation of the aromatic segments in favor of a tilted orientation. Except for Y17, the limiting cross-sectional areas of the other three molecules are slightly shifted to higher surface areas with increasing PEO length (Table 1). This result indicates that a portion of the benzene ring contacts the water surface and occupies more area as the PEO chains increase in length. Longer PEO chains serve as stronger anchors, probably by increasing the number of hydrogen bonds with the water molecules, thus creating a greater occupied area and more stable monolayers. Also, the Y21 molecule shows a significantly more extensive plateau than the Y34 and Y45 molecules. Based on the A_0 critical area values, the aromatic rings occupy a higher surface area upon compression as the PEO chain length increases (due to orientation toward the water surface). As the hydrophobic anchors occupy larger areas on the surface, their overlap upon compression will increasingly hinder the pancake-to-brush transition of the PEO chains, and the plateau region will become less distinct. Similar effects were observed for linear polystyrene (PS)-*b*-PEO chains as a function of spreading solution concentration due to differences in PS packing.[10]

Following the pseudoplateau, the surface pressure sharply increases at low molecular areas (above 40–60 mN m^{-1}), which indicates that the film is more rigid toward compression. At this point, a pure PEO monolayer of such chains would dissolve in water. The presence of the aromatic segments, however, anchors the PEO chains, thus leading to higher surface pressures. Therefore, the sharply increased isotherms of the three molecules seem to primarily reflect strong repulsive interactions of hydrophobic components within the highly compressed monolayer. Instead, the same aromatic segment of each molecule leads to similar behavior in a highly compressed state (after the pseudoplateau region).

2.2. Transferred Films on a Solid Support

Monolayers of the Y-shaped molecules transferred onto silicon substrates at a low surface pressure of 0.5 mN m^{-1} show smooth and featureless films on macroscopic scans, except for that of the Y17 molecule which reveals the formation of irregular aggregates (Figure S1 in the Supporting Information). For the Y21, Y34, and Y45 molecules, higher magnifications reveal globular domains that become larger as the PEO length increases (Figure S1). The shape of the globules results from desorption of the PEO chains. For the Y45 molecule, besides the individual globules, some larger clumps were also observed. This is most probably due to entanglement of the longest PEO chains at the air/water interface upon compression.

On deposition of LB films at high surface pressure, for the Y17 molecule the shape of the aggregates has no noticeable changes except that it becomes more dense. This is in agreement with the *p*–*A* isotherm data, which show that the observed surface pressure monotonously increases mainly as a result of crowding of the aggregates upon compression (Figure 2, Figure S2 in the Supporting Information). The Y45 molecule revealed the formation of 2D circular domains (Figure S3 in the Supporting Information). These may be caused by entanglement of the longest PEO chains at the air/water interface.[7b] For the Y21 and Y34 molecules, films deposited before the monolayer collapse show a distinct morphology formation, as will be discussed below.

Y21 monolayers deposited onto mica substrates at different surface pressures revealed a variety of surface morphologies (Figure 3). Isolated, straight cylinders were formed at the low surface pressure of 2 mN m^{-1} with a uniform width of 40–50 nm and a length in the range from 300 to 400 nm. The individual cylinders are not stable and are prone to combine into bundles, indicative of a local orientational ordering. Also, the cylinders connected to the bundles seem to have special directions (Figure 3a). At slightly high surface pressure, there appeared a loosely interwoven morphology consisting of long cylinders and junctions formed by interconnection of three or four cylinders (Figure 3b). Further compression leads to interwoven morphologies with more densely packed and larger planar domains formed locally. Eventually, a vortical morphology covering a large surface area was observed (Figure 3d). In this state, the cylinders cannot preserve their identity and merge into large domains at a high density of molecular packing. Cross-sectional analysis shows that the heights of all the morphologies are almost unchanged from 2.8 to 3.2 nm, which demonstrates that the morphological evolution only occurred in a 2D manner.

Notably, the LB films of Y21 deposited on silicon substrates also show the formation of cylinders but do not align them along a certain orientation, while deposition onto mica substrates exhibits an interesting vortical morphology at high surface pressures. This indicates that the substrate may play a critical role during the film transformation. Oriented structures of

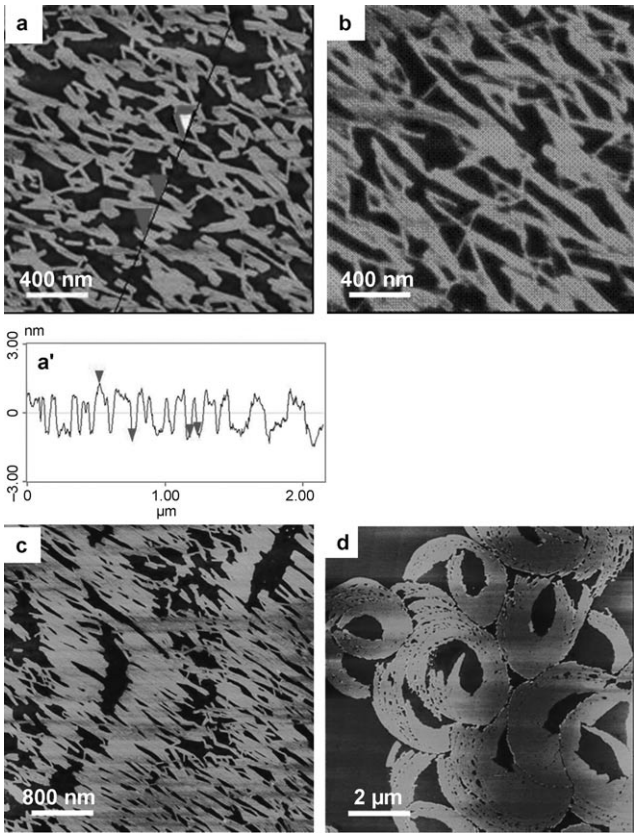

Figure 3. AFM topographical images of Y21 deposited onto freshly cleaved mica substrates at a surface pressure of a) 2 mN m^{-1}, scan size 2×2 μm, *z* range 6 nm; b) 3 mN m^{-1}, scan size 2×2 μm, *z* range 5 nm; c) 5 mN m^{-1}, scan size 4×4 μm, *z* range 5 nm; d) 8 mN m^{-1}, scan size 10×10 μm, *z* range 6 nm. a') Height profiles along the corresponding black line in (a).

π-conjugated polymers on mica substrates have also been reported.[27–30] Akutagawa et al. indicated that nanowires are oriented along the direction of the metal-ion array on a mica surface with sixfold symmetry during transformation of the film.[27] Li et al. reported a rod–coil molecule containing a PEO block with seven repeating units similar to 18-crown-6, which is capable of recognizing a K^+ cation array on the mica surface with sixfold symmetry.[28] In our case, the number of ethylene oxide repeating units of the Y21 molecule is three times that of the rod–coil molecule reported by Li et al., and the PEO block with 21 repeating units could also interact with K^+ cations according to the sixfold symmetry axes of the mica substrate. Indeed, the individual cylinders arranged along specific directions form angles of 60 and 120° with cylindrical bundles at slightly low surface pressure (Figure 3a and b). However, the force between the PEO and mica substrate is too weak to align the cylindrical bundles along preferred directions during transformation of the monolayer. The formation of the vortical morphology would start from cylinders along specific directions and then follow the subsequent assembly due to a cooperative interaction, in addition to the influence of water evaporation during the transfer process. These interactions consist of π–π stacking of the intermolecules, hydrophobic interactions between the alkyl chains, and interactions between the PEO block and the crystalline mica surface which has sixfold symmetry. The collective effect of these interactions and a subtle balance among them leads to the alignment of the domains and formation of the vortical morphology.

The Y34 molecule with a longer PEO chain than Y21 shows the formation of close-packed cylinders (Figure 4). At low surface pressures, short cylinders appeared that were irregularly arranged on the silicon wafer. Upon compression, the cylinders became longer (Figure 4b). High-resolution AFM images revealed that the cylinders are composed of several ridges parallel to the long axis of the cylinder. A detailed analysis of these cylindrical nanostructures revealed that the average distance between the ridges is about 14.4 nm and the height is about 1.7 nm, which accounts for the tip dilation[31] (Figure 4c, Figure S4 in the Supporting Information). As the surface pressure increased, the length of the cylinders increased to 1 μm; however, the height of the cylinders stayed approximately unchanged. In this state, the close-packed cylinders can still preserve their identity in the vicinity of the monolayer collapse.

To interpret these data and suggest an appropriate model of molecular packing within the two kinds of cylinders formed by the Y21 and Y34 molecules, UV/Vis and FTIR spectroscopy experiments were performed. Figure 5 shows the UV/Vis spectra of LB films of Y21 and Y34 transferred from the air/water interface at low and high surface pressures. It can be seen that there is a blue shift (from 298 to 284 nm for Y21 and from 292 to 283 nm for Y34) in LB films deposited at high surface pressure compared with the films deposited at low surface pressure. Both theoretical[32] and experimental[33] reports in the literature suggest that small aggregates of from two to six π-conjugated molecules can alter the absorption and fluorescence spectra of the isolated chromophore, thus leading to blue-shifted absorption and red-shifted emission. In our case, the blue-shifted spectra for the film deposited at high surface pressure compared with the film deposited at low surface pressure are attributed to the formation of H aggregates, in which the long axes of the molecules are aligned in a general face-to-face arrangement.[34] This finding is in agreement with the *p–A* isotherm measurements, where the aromatic rings are suggested to have a vertical arrangement.[35]

To further confirm the average orientation of the alkyl chains in the cylindrical structures, FTIR spectroscopic experiments were performed (Figure 6). A weak feature near 2953 cm^{-1} is assigned to the CH_3 asymmetric stretching mode of the hydrocarbon tail for all transferred films. In the LB films transferred at a low surface pressure of 0.5 mN m^{-1}, strong asymmetric and symmetric CH_2 stretching vibrations are observed at 2920 and 2851 cm^{-1} for the Y21 and 2920 and 2850 cm^{-1} for the Y34 molecules, respectively, whereas they are observed at 2918 and 2850 cm^{-1} in the LB films transferred at a surface pressure of 8 mN m^{-1} for the Y21 and 10 mN m^{-1} for the Y34 molecules. It is well known that the appearance of the CH_2 asymmetric and symmetric stretching bands at higher wavenumbers is indicative of conformational disorder in the hydrocarbon chains, whereas their appearance at lower wavenumbers (ca. 2918 and 2850 cm^{-1}, respectively) indicates an increased order and well-organized arrangement of the hydro-

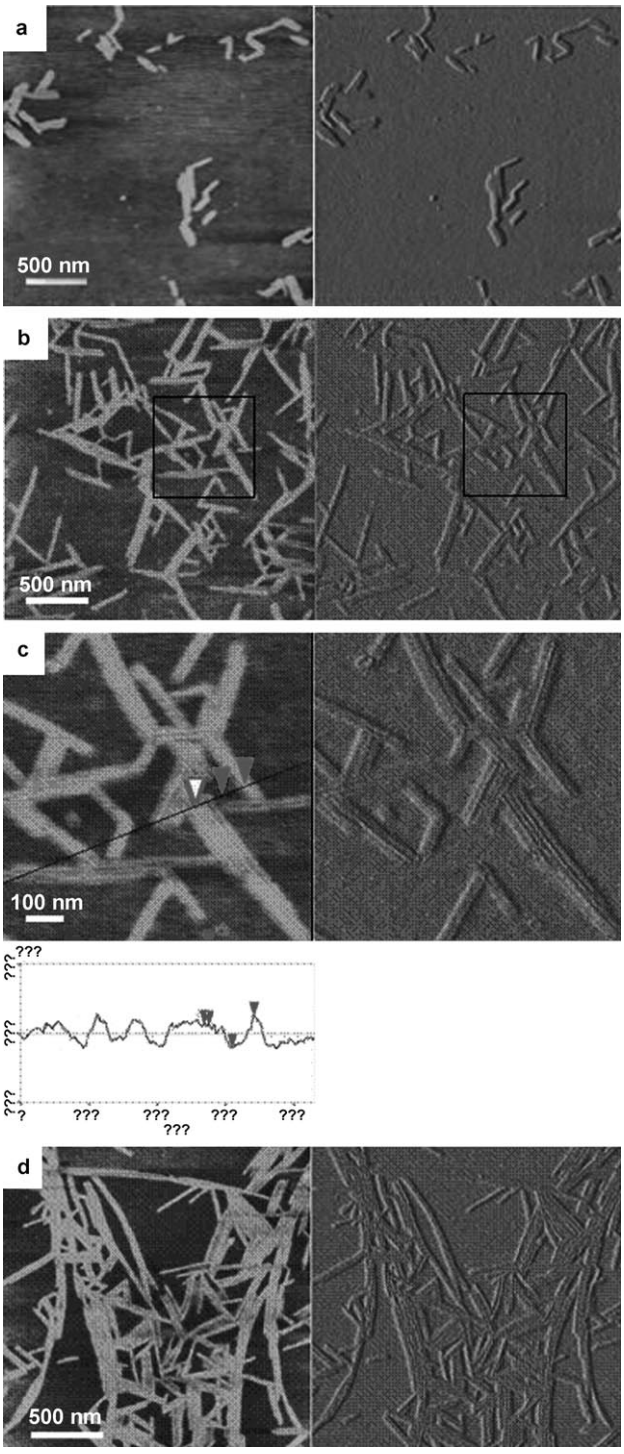

Figure 4. AFM images of Y34 deposited onto silicon substrates at a surface pressure of a) 5, b) 8, and d) 10 mN m^{-1}; c) High-resolution images of part of the area shown as a square in (b) and the corresponding cross-sections of the close-packed cylindrical structure (no scale bar, there are some question marks in the cross-sectional graph); the *z* range for the topography (left) is 6 nm, whereas that for the phase (right) is 0.2 v.

carbon chains.[36,37c] In the present case, the vibrational position of the films transferred at high surface pressure suggests that the alkyl chains are basically in an ordered packing. Also, the relative intensity of the asymmetric CH_2 to symmetric vibration increases in LB films of the Y34 molecule compared with that of the Y21 molecule, which indicates that the alkyl chains are more inclined to the substrate surface in the LB films of Y34 than in that of Y21 transferred at high surface pressure.[37,38]

2.3. Molecular Modeling

The combined analysis of the *p–A* isotherm data for the molecular areas, the AFM images of the cylinder dimensions, the UV/Vis data on the benzene ring packing, the FTIR data on the alkyl chain orientation, and the molecular dimensions from minimized molecular models allowed us to suggest a model of the molecular packing for a cylinder (see Figure 7). In this model, the Y21 molecule is aligned with face-to-face packing of the aromatic rings standing on the surface with a certain tilting angle. For the Y34 molecule, the architecture of the close-packed cylinders is described by the molecules being packed parallel to each other with the molecular axis of the aromatic backbone perpendicular to the long axis of the cylinder (Figure 7). The cylindrical height of the model proposed for the Y21 molecule is evaluated to be 2.7 nm, which fits well to the AFM data. The effective width of the neighboring ridge suggested in the model for the Y34 molecule is about 14.2 nm and the height is about 1.6 nm, which is very close to the experimental results as well.

It is well known that the surface behavior of amphiphilic molecules should depend strongly upon the amphiphilic balance of the hydrophobic and hydrophilic fragments and the freedom of their reorganization to adopt the proper orientation at the air/water interface, which is constrained by the chemical architecture. The mismatch of the cross-sectional areas of the PEO chain and the benzene ring with attached alkyl chains, and the higher PEO content of Y34 could lead to Y34 with a higher degree of tilting from the surface normal than Y21,[11a] although we could not deduce the exact tilting angle from our experimental data.

We suggest that deposited films in a "gas state" (isolated molecules at low surface pressure) could not preserve single-molecular freestanding conformations on the substrates due to no force supporting them. Upon compression, the strong intermolecular interaction of the Y21 molecule through π–π stacking could easily drive the molecule to form cylinders at the air/water interface, whereas for the Y34 molecule, the alkyl chains will contact first due to the higher tilting angle from the surface normal compared with that of Y21. In this state, the hydrophobic interactions between the alkyl chains will play a role. As a result, the molecules will move sideways and parallel to their neighbors due to π–π interaction, eventually leading to the formation of close-packed cylinders (Figure 7). This aggregation is so strong that it is preserved in the course of the flipping and formation of the cylindrical backbones.

2.4. General Discussion

The Y-shaped molecules with different PEO lengths exhibited different surface morphologies. Our experimental results suggested that the mismatch between the PEO and benzene ring

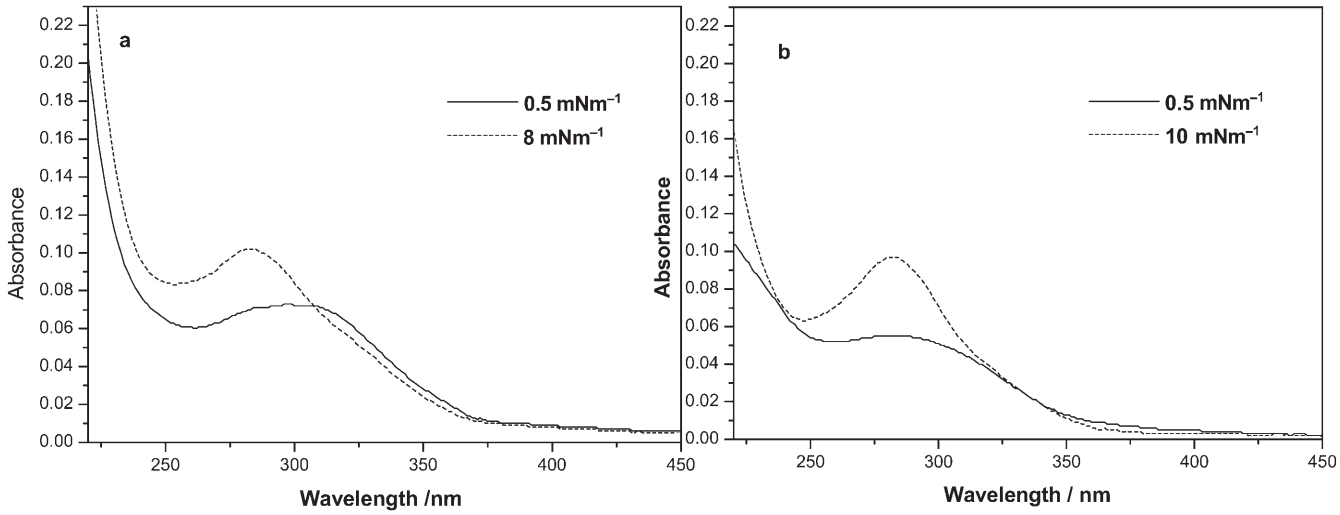

Figure 5. UV/Vis spectra of 20-layer LB films of Y21 (a) and Y34 (b) deposited on quartz plates.

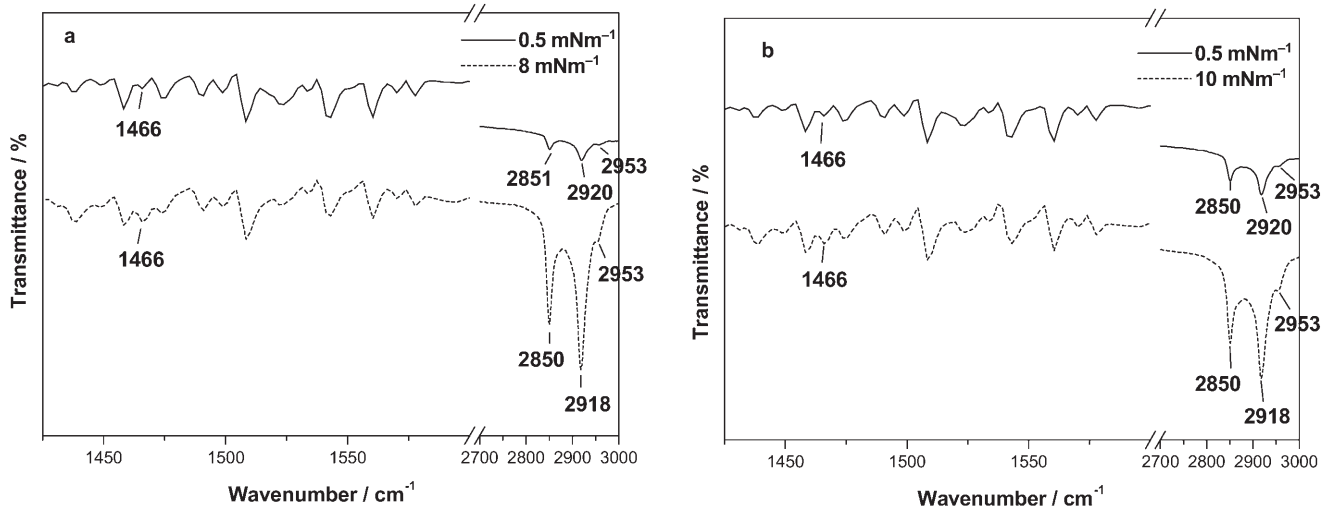

Figure 6. FTIR spectra of 30-layer LB films of Y21 (a) and Y34 (b) deposited on CaF_2 slides.

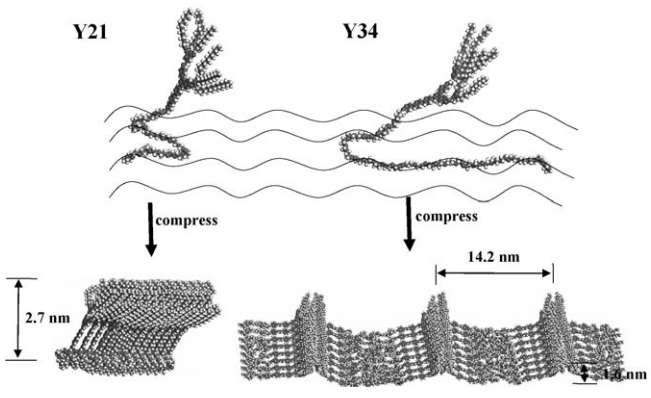

Figure 7. Model of the molecular packing of Y21 and Y34 at the air/water interface.

with alkyl chains, and the different PEO contents are crucial for the molecule arrangement at the air/water interface.[39] The molecular tilted orientation provides the appropriate balance between the cross-sectional area of the PEO block and the aromatic segment with alkyl chains.

For the Y17 molecule, since no micellar aggregates were present in the spreading solution (spreading solvent is chloroform), as confirmed by dynamic light scattering measurements, we conclude that initial aggregation takes place spontaneously at the air/water interface.[9] This can be explained by the fact that the aromatic segments cannot be tethered by PEO chains at the air/water interface due to the smaller volume fraction compared with the aromatic segments (Table 1).

For the other three molecules, note that we have not observed any indications of a phase transition from flat-on to

stand-off arrangements of the aromatic segments at different surface pressures. The fact that the aromatic benzene rings have hydrophobic tails attached to the PEO polar head at a single point provides the driving force for the stand-off orientation of the aromatic segments. Upon compression, due to the longest PEO entanglement and coiling, the Y45 molecule revealed the formation of 2D circular domains,[7b] whereas for Y21 and Y34, two kinds of cylindrical nanostructures were formed. Such associations are clearly caused by π–π interactions of the aromatic segments, hydrophobic interactions of the alkyl chains, and steric limitations on their packing under confined-space conditions. The cylinders were extremely stable during transfer, were not disrupted by scanning with high forces, and extended uninterrupted over several micrometers. In addition, the very particular internal organization of the close-packed cylinders with a hydrophobic ridge and a hydrophilic concave area makes them an intriguing candidate for the templating of inorganic wired nanostructures, similar to that already demonstrated for rigid molecules.[40] This work provides a clue to the design of amphiphilic molecular architectures to control nanostructures at the air/water interface.

3. Conclusions

We have studied the interfacial behavior of Y-shaped rod–coil molecules with different PEO lengths at various compression stages by an LB balance and morphology study. For the Y17 molecule, initial aggregation occurred spontaneously at the air/water interface, whereas for the other three molecules, the isotherms presented a pseudoplateau at a surface pressure of 8–10 mN m^{-1}. Transferred monolayers revealed two kinds of cylindrical nanostructures formed for the Y21 and Y34 molecules before monolayer collapse. The mismatch between the PEO and benzene ring with alkyl chains, and the different PEO contents provide the force for molecular arrangement at the air/water interface. Such associations are caused by π–π interactions of the aromatic segments, hydrophobic interactions of the alkyl chains, and steric limitations on their packing under confined-space conditions. Due to the longest PEO chain entanglement and coiling, Y45 revealed the formation of 2D circular domains. Additionally, a vortical morphology was obtained for Y21 on a mica substrate, which indicates that the substrate chemistry affects the morphologies during the film-transfer process.

Acknowledgements

This work was supported by the National Creative Research Initiative Program. The BK21 program from the Ministry of Education and Human Resources Development is gratefully acknowledged.

Keywords: interfaces · monolayers · nanostructures · rod–coil molecules · stacking interactions

[1] A. Ulman, *An Introduction to Ultrathin Organic Film: From Langmuir–Blodgett to Self-Assembly*, Academic Press, Boston, **1991**.
[2] a) K. Albrecht, A. Mourran, M. Moeller, *Adv. Polym. Sci.* **2006**, *200*, 57–70; b) A. E. Hosoi, D. Kogan, C. E. Devereaux, A. J. Bernoff, S. M. Baker, *Phys. Rev. Lett.* **2005**, *95*, 037801.
[3] a) J. R. Lu, T. J. Su, R. K. Thomas, J. Penfold, R. W. Richards, *Polymer* **1996**, *37*, 109–114; b) E. P. K. Currie, F. A. M. Leermakers, M. A. C. Stuart, G. J. Fleer, *Macromolecules* **1999**, *32*, 487–498; c) M. G. Muñoz, F. Monroy, F. Ortega, R. G. Rubio, D. Langevin, *Langmuir* **2000**, *16*, 1083–1093.
[4] a) A. Wesemann, H. Ahrens, R. Steitz, S. Förster, C. A. Helm, *Langmuir* **2003**, *19*, 709–716; b) A. Wesemann, H. Ahrens, S. Förster, C. A. Helm, *Langmuir* **2004**, *20*, 11528–11535; c) K. Busse, C. Peetla, J. Kressler, *Langmuir* **2007**, *23*, 6975–6982.
[5] a) Z. Xu, N. B. Holland, R. E. Marchant, *Langmuir* **2001**, *17*, 377–383; b) T. R. Baekmark, G. Elender, D. D. Lasic, E. Sackmann, *Langmuir* **1995**, *11*, 3975–3987.
[6] a) C. Barentin, P. Muller, J. F. Joanny, *Macromolecules* **1998**, *31*, 2198–2211; b) C. Barentin, J. F. Joanny, *Langmuir* **1999**, *15*, 1802–1811.
[7] a) R. B. Cheyne, M. G. Moffitt, *Langmuir* **2005**, *21*, 5453–5460; b) J. L. Logan, P. Masse, B. Dorvel, A. M. Skolnik, S. S. Sheiko, R. Francis, D. Taton, Y. Gnanou, R. S. Duran, *Langmuir* **2005**, *21*, 3424–3431.
[8] a) S. M. Baker, K. A. Leach, C. E. Devereaux, D. E. Gragson, *Macromolecules* **2000**, *33*, 5432–5436; b) C. E. Devereaux, S. M. Baker, *Macromolecules* **2002**, *35*, 1921–1927.
[9] J. K. Cox, K. Yu, B. Constantine, A. Eisenberg, R. B. Lennox, *Langmuir* **1999**, *15*, 7714–7718.
[10] R. B. Cheyne, M. G. Moffitt, *Langmuir* **2006**, *22*, 8387–8396.
[11] a) K. L. Genson, D. Vaknin, O. Villacencio, D. V. McGrath, V. V. Tsukruk, *J. Phys. Chem. B* **2002**, *106*, 11277–11284; b) M. Ornatska, S. Peleshanko, K. L. Genson, B. Rybak, K. N. Bergman, V. V. Tsukruk, *J. Am. Chem. Soc.* **2004**, *126*, 9675–9684; c) O. Y. Mindyuk, P. A. Heiney, *Adv. Mater.* **1999**, *11*, 341–344.
[12] S. I. Stupp, V. LeBonheur, K. Walker, L. S. Li, K. E. Huggins, M. Keser, A. Amstutz, *Science* **1997**, *276*, 384–389.
[13] a) M. Lee, B.-K. Cho, W.-C. Zin, *Chem. Rev.* **2001**, *101*, 3869–3892; b) J.-K. Kim, E. Lee, Z. Huang, M. Lee, *J. Am. Chem. Soc.* **2006**, *128*, 14022–14023.
[14] a) M. Lee, J.-W. Kim, S. Peleshanko, K. Larson, Y.-S. Yoo, D. Vaknin, S. Markutya, V. V. Tsukruk, *J. Am. Chem. Soc.* **2002**, *124*, 9121–9128; b) V. V. Tsukruk, K. Genson, S. Peleshanko, S. Markutsya, M. Lee, Y.-S. Yoo, *Langmuir* **2003**, *19*, 495–499; c) J. Holzmueller, K. L. Genson, Y. Park, Y.-S. Yoo, M.-H. Park, M. Lee, V. V. Tsukruk, *Langmuir* **2005**, *21*, 6392–6398; d) L. Liu, K.-S. Moon, R. Gunawidjaja, E. Lee, V. V. Tsukruk, M. Lee, *Langmuir* **2008**, *24*, 3930–3936.
[15] J. Zhang, H. Q. Cao, X. H. Wan, Q. F. Zhou, *Langmuir* **2006**, *22*, 6587–6592.
[16] a) Y. Park, Y.-W. Choi, S. Park, C. S. Cho, M. J. Fasolka, D. Sohn, *J. Colloid Interface Sci.* **2005**, *283*, 322–328; b) N. A. J. M. Sommerdijk, S. J. Holder, R. C. Hiorns, R. G. Jones, R. J. M. Nolte, *Macromolecules* **2000**, *33*, 8289–8294; c) C.-S. Cho, A. Kobayashi, M. Goto, T. Akaike, *Thin Solid Films* **1995**, *264*, 82–88.
[17] J.-K. Kim, M.-K. Hong, J.-H. Ahn, M. Lee, *Angew. Chem.* **2005**, *117*, 332–336; *Angew. Chem. Int. Ed.* **2005**, *44*, 328–332.
[18] S. Szunerits, R. Boukherroub, *Langmuir* **2006**, *22*, 1660–1663.
[19] S. N. Magonov, V. Elings, M.-H. Whangbo, *Surf. Sci.* **1997**, *375*, L385–L391.
[20] S. N. Magonov, *Surface Analysis with STM and AFM: Experimental and Theoretical Aspects of Image Analysis*, VCH, Weinheim, **1996**.
[21] a) A. M. Gonçalves da Silva, E. J. M. Filipe, J. M. R. d'Oliveira, J. M. G. Martinho, *Langmuir* **1996**, *12*, 6547–6553; b) A. M. Gonçalves da Silva, A. L. Simões Gamboa, J. M. G. Martinho, *Langmuir* **1998**, *14*, 5327–5330.
[22] M. C. Fauré, P. Bassereau, L. T. Lee, A. Menelle, C. Lheveder, *Macromolecules* **1999**, *32*, 8538–8550.
[23] H. D. Bijsterbosch, V. O. de Haan, A. W. de Graaf, M. Mellema, F. A. M. Leermakers, M. A. Cohen Stuart, A. A. van Well, *Langmuir* **1995**, *11*, 4467–4473.
[24] a) J. K. Cox, K. Yu, A. Eisenberg, R. B. Lennox, *Phys. Chem. Chem. Phys.* **1999**, *1*, 4417–4421; b) S. Rivillon, M. G. Muñoz, F. Monroy, F. Ortega, R. G. Rubio, *Macromolecules* **2003**, *36*, 4068–4077.
[25] M. C. Fauré, P. Bassereau, M. A. Carignano, I. Szleifer, Y. Gallot, D. Andelman, *Eur. Phys. J. B* **1998**, *3*, 365–375.

[26] B. B. Sauer, H. Yu, *Macromolecules* **1989**, *22*, 786–791.
[27] T. Akutagawa, T. Ohta, T. Hasegawa, T. Nakamura, C. A. Chistensen, J. Becher, *Proc. Natl. Acad. Sci. USA* **2002**, *99*, 5028–5033.
[28] H. B. Li, Q. T. Liu, M. Xu, W. F. Bu, X. K. Lin, L. X. Wu, J. C. Shen, *J. Phys. Chem. B* **2005**, *109*, 2855–2861.
[29] a) P. Samorí, V. Francke, K. Müllen, J. P. Rabe, *Thin Solid Films* **1998**, *336*, 13–15; b) P. Samorí, V. Francke, K. Müllen, J. P. Rabe, *Chem. Eur. J.* **1999**, *5*, 2312–2317.
[30] J. Xu, C.-Z. Zhou, L. H. Yang, N. T. S. Chung, Z.-K. Chen, *Langmuir* **2004**, *20*, 950–956.
[31] P. Samorí, V. Francke, T. Mangel, K. Müllen, J. P. Rabe, *Opt. Mater.* **1998**, *9*, 390–393.
[32] J. Cornil, D. A. dos Santos, X. Crispin, R. Silbey, J. L. Brédas, *J. Am. Chem. Soc.* **1998**, *120*, 1289–1299.
[33] X. Song, C. Geiger, M. Farahat, J. Perlstein, D. G. Whitten, *J. Am. Chem. Soc.* **1997**, *119*, 12481–12491.
[34] a) W. Yang, X. Chai, L. Chi, X. Liu, Y. Cao, R. Lu, Y. Jiang, X. Tang, H. Fuchs, T. Li, *Chem. Eur. J.* **1999**, *5*, 1144–1149; b) A. Ajayaghosh, S. J. George, *J. Am. Chem. Soc.* **2001**, *123*, 5148–5149; c) X. Huang, C. Li, S. Jiang, X. Wang, B. Zhang, M. Liu, *J. Am. Chem. Soc.* **2004**, *126*, 1322–1323; d) P. Guo, L. Zhang, M. Liu, *Adv. Mater.* **2006**, *18*, 177–180.
[35] L. Chen, C. Geiger, J. Perlstein, D. G. Whitten, *J. Phys. Chem. B* **1999**, *103*, 9161–9167.
[36] a) H. Sapper, D. G. Cameron, H. H. Mantsch, *Can. J. Chem.* **1981**, *59*, 2543–2549; b) D. G. Cameron, A. Martin, D. J. Moffatt, H. H. Mantsh, *Biochemistry* **1985**, *24*, 4355–4359.
[37] a) M. Kubota, Y. Ozaki, T. Araki, S. Ohki, K. Iriyama, *Langmuir* **1991**, *7*, 774–778; b) S. Terashita, K. Nakatsu, Y. Ozaki, T. Mochida, T. Araki, K. Iriyama, *Langmuir* **1992**, *8*, 3051–3056; c) S. Terashita, Y. Ozaki, K. Iriyama, *J. Phys. Chem.* **1993**, *97*, 10445–10452; d) A. Nakagoshi, S. Terashita, Y. Ozaki, *Langmuir* **1994**, *10*, 779–783; e) A. Nakagoshi, Y. Wang, Y. Ozaki, K. Iriyama, *Langmuir* **1995**, *11*, 3610–3616.
[38] Another peak is observed at 1466 cm^{-1} which is attributed to the CH_2 scissoring mode of alkyl chains. This band does not split while keeping a single band in all LB films of Y21 and Y34, which is indicative of triclinic subcell packing of alkyl chains in multilayer LB films of Y21 and Y34 (F. Kimura, J. Umemura, T. Takenaka, *Langmuir* **1986**, *2*, 96–101).
[39] a) G. Weidemann, G. Brezesinki, D. Vollhardt, H. Mohwald, *Langmuir* **1998**, *14*, 6485–6492; b) G. Weidemann, G. Brezesinki, D. Vollhardt, C. DeWolf, H. Mohwald, *Langmuir* **1999**, *15*, 2901–2910; c) E. B. Sirota, *Langmuir* **1997**, *13*, 3849–3859.
[40] a) S. S. Sheiko, M. Moller, *Chem. Rev.* **2001**, *101*, 4099–4124; b) R. Djalali, S.-Y. Li, M. Schmidt, *Macromolecules* **2002**, *35*, 4282–4288.

Received: March 5, 2008
Revised: April 22, 2008
Published online on July 10, 2008

